Bol. Soc. Paran. Mat.
©SPM – E-ISSN-2175-1188
SPM: www.spm.uem.br/bspm

(3s.) **v. 2025 (43)** : 1–14.
ISSN-0037-8712
doi:10.5269/bspm.76511

Improved Perona-Malik Model with a Leray-Lions Operator for Image Denoising

S.M. Douiri, H. Farjil*, and M. Moumni

ABSTRACT: In the current paper, we introduce an extended framework for image denoising. The formulated diffusion model integrates both the Perona-Malik and a Leray-Lions's type operator, aiming to achieve both effective noise suppression and preservation of important image features. We first explore the proposed model mathematically, determining whether solutions exist and are unique. Then, we demonstrate the model's applicability for image noise reduction, by providing various numerical simulations.

Key Words: Non-linear parabolic problems, existence and uniqueness of solutions, image denoising, finite difference methods.

Contents

1. Introduction

In recent years, there has been a noticeable shift in mathematicians' focus towards the areas of visual information enhancement and digital image analysis, indicating a growing interest in these domains. A significant challenge within this field is image restoration, propelled by the proliferation of digital images and videos captured under various conditions, often resulting in noise-corrupted images. Image denoising, a fundamental task in image restoration, aims to recover the underlying information from noisy images. In typical scenarios, an image comprising (N, M) pixels can be effectively modeled as:

$$f(r,s) = u(r,s) + I(r,s) \quad \text{where} \quad r = 1,\dots,N \quad \text{and} \quad s = 1,\dots,M,$$

with $f(r,s)$ denotes the (r^{th}, s^{th}) pixel of the observed noisy image, $u(r,s)$ represents the true image information, and $I(r,s)$ indicates the presence of noise affecting each pixel.
In the realm of image processing, the primary goal of image denoising is to effectively remove unwanted noise thus simultaneously preserving and restoring the essential features and intricate details present in the image. This task is crucial as noisy images can obscure vital information and degrade the overall quality of visual content [7,18]. Over recent years, the demand for efficient denoising techniques has surged, driven by the proliferation of digital imaging technologies and the increasing prevalence of noise-corrupted images captured under diverse conditions [14]. To address this challenge, various methodologies have been developed, with approaches rooted in nonlinear diffusion and variational models leveraging partial differential equations emerging as particularly prominent [4,9,16,17]. Nonlinear diffusion techniques focus on the controlled diffusion of image intensities to smoothen noisy regions while preserving edges and structural details. Similarly, variational models formulate denoising as an optimization problem, seeking to minimize a carefully crafted objective function that balances fidelity to the original image with the suppression of noise artifacts. These methods have garnered significant attention and adoption due to their ability to yield impressive denoising results across a wide range of image types and noise characteristics,

* Corresponding author: hindfarjil@gmail.com.
2020 *Mathematics Subject Classification:* 35K55, 94A08, 68U10, 65M06.
Submitted April 23, 2025. Published September 23, 2025

making them indispensable tools in modern image processing applications. Certainly, the Perona-Malik model, a pioneering contribution in the realm of image processing, offers a sophisticated solution to the ubiquitous problem of image denoising and edge enhancement [15]. Proposed by Pietro Perona and Jitendra Malik in 1990, this model harnesses the power of partial differential equations to achieve remarkable results in preserving image characteristics while efficiently reducing noise. The Euler-Lagrange equation associated to the energy for the functional of Perona-Malik was offered by

$$u - \operatorname{div}\left(g(|\nabla u|)\nabla u\right) = f \quad \text{on } \Omega,$$

where $g(.)$ is a decreasing non-negative function such that $g(0) = 1$ and $\lim_{r\to\infty} g(r) = 0$. The function $g(.)$ is also utilized as an edge detection operator, designed to identify key pixels that are critical for preserving important structures within the image. By detecting these edges, the denoising process can be applied more effectively, allowing for smoother transitions while minimizing the loss of essential details. This enables the model to selectively preserve edges, ensuring that the denoising process enhances the image without introducing artifacts or blurring important features. The model offers one of two types expressions of g :

$$g(r) = \exp\left(-\frac{r^2}{2\lambda^2}\right) \text{ or } \quad g(r) = \frac{1}{1 + \left(\frac{r}{\lambda}\right)^2}, \quad \text{where } \quad \lambda > 0.$$

Yet, the Perona-Malik approach exhibits two significant limitations: the "paradoxical result" due to the ill-posed nature of the problem and the "staircase effect" which causes the blocky images, observed during numerical simulations [12,8]. Catte et al.'s regularization of the Perona-Malik model represents an important advancement in the field of image processing [8], offering a promising solution to the paradoxical result and the staircase effect. By incorporating additional constraints or penalties into the diffusion process, their approach enhances the model's ability to produce high-quality denoised images while preserving important structural information. For more details, we refer to [1,2,5,10,11]. To achieve the same goals, Atlas et al. in [3] dealt the existence and uniqueness of solution in a mathematical model, which, in addition to the operator used by Perona and Malik, included a p-Laplacian operator. The model they propose exactly as shown,

$$u - \operatorname{div}\left(g(|\nabla u|)\nabla u\right) - \frac{1}{\lambda^p}\operatorname{div}\left(|\nabla u|^{p-2}\nabla u\right) = f \quad \text{on } \Omega,$$

where $\lambda > 0$ and $p \geq 1+\lambda^2$. However, this model demonstrates a lack of robustness and remains susceptible to certain artifacts, including the presence of virtual edges. These artifacts manifest in various forms, such as the staircasing effect, which introduces unnatural block-like structures, and a noticeable loss of contrast, which reduces the clarity and sharpness of the reconstructed image. Such limitations hinder the overall performance and reliability of the model, particularly in applications requiring high-fidelity image processing.

Taking the preceding discussion into account, this paper aims to fix these drawbacks and also aims to extend the model proposed in [3] by substituting the p-Laplacian operator with an operator of the Leray-Lions type, it's basically reliant on ∇u and x. More specifically, we will address the following problem,

$$(\mathcal{P}) \begin{cases} u + A(u) - \operatorname{div}\left(g(|\nabla u|)\nabla u\right) = f \quad \text{in } \Omega, \\ \\ \left(a(., \nabla u) + g(|\nabla u|)\nabla u\right)\vec{n} = 0 \quad \text{in } \partial\Omega. \end{cases} \tag{1.1}$$

In this context, Ω represents a bounded open subset of $\mathbb{R}^N$ $(N \geq 2)$, $f \in L^\infty(\Omega)$ and $A(u) := -\operatorname{div} a(., \nabla u)$ where $(x, \zeta) \longmapsto a(x, \zeta)$ is a function of Carathéodory from $\Omega \times \mathbb{R}^N$ to $\mathbb{R}^N$. In the theoretical section, inspired by the approach in [3], we use the monotonicity method to prove that, under appropriate growth, coercivity, and monotonicity conditions, there exists a unique weak solution to our problem. So we assume, for a.e. $x \in \Omega$ and all $\zeta \neq \zeta^* \in \mathbb{R}^N$, the following hypotheses,

$$|a(x, \zeta)| \leq \frac{k(x)}{\lambda^p}|\zeta|^{p-1}; \tag{1.2}$$

$$[a(x,\zeta) - a(x,\zeta^*)] \cdot [\zeta - \zeta^*] > 0; \tag{1.3}$$

$$a(x,\zeta) \cdot \zeta \geq \frac{\alpha}{\lambda^p}|\zeta|^p, \tag{1.4}$$

where $\alpha > 0$ and $k(.)$ belongs to $L^\infty(\Omega)$ such that $0 < \alpha_1 \leq k(x) \leq \alpha_2$ for a.e. $x \in \Omega$.
In the numerical section, applying our approach to three examples of Carathéodory functions allows us to regularize the Perona-Malik model. These can be noted $a_i(x,\zeta)$, $i = 1, 2, 3$, and presented as follows:

$$a_1(x,\zeta) = \frac{\alpha - \exp\left(-\frac{|\zeta|^2}{2\lambda^2}\right)}{\lambda^p}|\zeta|^{p-2}\zeta, \text{ with } \alpha > 1.$$

$$a_2(x,\zeta) = \frac{\max\left(\frac{1}{1+\left(\frac{|\zeta|}{\lambda}\right)^2}, 1 - \exp\left(-\frac{|\zeta|^2}{2\lambda^2}\right)\right)}{\lambda^p}|\zeta|^{p-2}\zeta.$$

$$a_3(x,\zeta) = \frac{\alpha + \frac{1}{1+\left(\frac{|\zeta|}{\lambda}\right)^2}}{\lambda^p}|\zeta|^{p-2}\zeta, \text{ with } \alpha > 0.$$

Similar to the approach of Perona and Malik [15] and Atlas et al. [3], our model incorporates a novel edge detection operator that enhances the denoising process while leveraging the diffusivity function of Perona-Malik. To validate this assumption, Fig. 1 presents an experiment using the *Cameraman* image, where we analyze the detected edges by applying three different edge detection operators, denoted as a_1, a_2 and a_3. This comparison aims to illustrate the effectiveness of our proposed operator in preserving important structural details while mitigating noise.

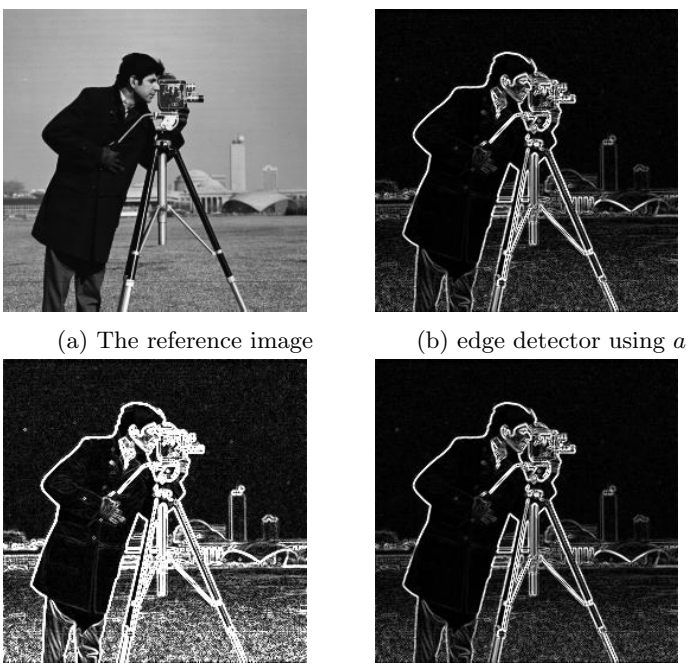

(a) The reference image (b) edge detector using a_1

(c) edge detector using a_2 (d) edge detector using a_3

Figure 1: Edge detector of the *Cameraman* image using a_1, a_2 and a_3.

Based on the figure above and the computed PSNR values for the three aforementioned models, our proposed model, RPM (Regularized Perona-Malik), demonstrates superior performance compared to the PMPL (Perona-Malik combined with the p-Laplacian operator) model [3]. Specifically, RPM is more effective in mitigating the staircasing effect while preserving finer image details, leading to improved overall reconstruction quality.

Beyond the promising modeling choices involved in employing the Carathéodory functions a_i we also establish the well-posedness of the proposed model 1.1 by leveraging a key lemma. Additionally, we utilize standard analytical tools, including the Minty-Browder theorem [6] and the Rellich-Kondrachov theorem, to reinforce our theoretical framework.

To further deepen the mathematical analysis, we provide an asymptotic study of the key parameter p which plays a central role in our model $(\mathcal{P})$ as formulated in Eq. 1.1. By applying the finite difference method, we implemented a numerical scheme for the proposed model to validate the theoretical results and demonstrate the superiority and robustness of our approach. However, a significant challenge lies in the presence of multiple parameters, which makes their adjustment a complex task in order to achieve optimal results. The sensitivity of these parameters can significantly influence the models performance, particularly in terms of stability, accuracy, and computational efficiency. To overcome this difficulty, we adopt a systematic approach to determine the optimal parameter values. Specifically, we identify the best-performing configurations by selecting those that maximize the Peak Signal-to-Noise Ratio (PSNR), a widely used metric for assessing image quality. This optimization process ensures that our model not only minimizes artifacts such as the staircasing effect but also enhances detail preservation, thereby improving the overall effectiveness of the proposed framework.

The remainder of this paper is organized as follows. Section 2 establishes the existence and uniqueness of a solution to problem $(\mathcal{P})$ by leveraging a specific lemma. Section 3 investigates the influence of the key parameter p on the model's behavior, precisely in its asymptotic behavior $p \to \infty$. Section 4 provides a numerical validation of the proposed approach in the context of image denoising, comparing its performance against several state-of-the-art models. Finally, Section 5 concludes with a summary of the findings and additional insights into potential future developments.

2. Mathematical standpoint

To establish the existence and uniqueness of a solution, we analyze the function b and the next lemma, which play a crucial role in the theoretical formulation of the problem. Evaluating b allows us to determine the necessary conditions for ensuring well-posedness, thereby laying the foundation for rigorous mathematical justification.

Let us consider the following function $b : \mathbb{R}^N \to \mathbb{R}^N$, defined as

$$b(\zeta) = g(|\zeta|)\zeta + a(x, \zeta) \quad \forall \zeta \in \mathbb{R}^N.$$

In order to confirm proof for the existence and singularness result of $(\mathcal{P})$ model, we make use of the accompanying lemma.

Lemma 2.1 *Let $p \geq 1 + \frac{\lambda^2}{\alpha}$. For any $\zeta, \nu \in \mathbb{R}^N$ in order that $\zeta \neq \nu$ we have after the previous line*

$$(b(\zeta) - b(\nu))(\zeta - \nu) > 0.$$

Proof:

$$\begin{aligned}(b(\zeta) - b(\nu))(\zeta - \nu) &= (g(|\zeta|)\zeta + a(x, \nabla\zeta) - g(|\nu|)\nu - a(x, \nabla\nu))(\zeta - \nu) \\ &\geq |\zeta|^2 g(|\zeta|) - g(|\zeta|)|\zeta||\nu| + a(x, \zeta)\zeta - |a(x, \zeta)||\nu| \\ &\quad - g(|\nu|)|\nu||\zeta| + |\nu|^2 g(|\nu|) - |a(x, \nu)||\zeta| + a(x, \nu)\nu.\end{aligned}$$

By using (1.4) and (1.2), we gain

$$\begin{aligned}(b(\zeta)-b(\nu))\,(\zeta-\nu) &\geq g(|\zeta|)|\zeta|^2 - g(|\zeta|)|\zeta||\nu| - g(|\nu|)|\nu||\zeta| + g(|\nu|)|\nu|^2 \\ &\quad + \frac{\alpha}{\lambda^p}|\zeta|^p - k(x)|\zeta|^{p-1}|\nu| - k(x)|\nu|^{p-1}|\zeta| + \frac{\alpha}{\lambda^p}|\nu|^p \\ &\geq (g(|\zeta|)|\zeta| - g(|\nu|)|\nu|)\,(|\zeta|-|\nu|) + \frac{\alpha}{\lambda^p}|\zeta|^p + \frac{\alpha}{\lambda^p}|\nu|^p \\ &\quad - \frac{\alpha}{\lambda^p}|\zeta|^{p-1}|\nu| - \frac{\alpha}{\lambda^p}|\nu|^{p-1}|\zeta| \\ &\geq (g(|\zeta|)|\zeta| - g(|\nu|)|\nu|)\,(|\zeta|-|\nu|) + \frac{\alpha|\zeta|^{p-1}}{\lambda^p}(|\zeta|-|\nu|) \\ &\quad - \frac{\alpha|\nu|^{p-1}}{\lambda^p}(|\zeta|-|\nu|), \\ &\geq \left(g(|\zeta|)|\zeta| + \frac{\alpha}{\lambda^p}|\zeta|^{p-1} - g(|\nu|)|\nu| - \frac{\alpha}{\lambda^p}|\nu|^{p-1}\right)(|\zeta|-|\nu|)\,.\end{aligned}$$

Verifying the monotonic behavior of the function H_λ, as suggested by the equation, is crucial to completing the proof

$$H_\lambda(t) = tg(t) + \frac{\alpha}{\lambda^p}t^{p-1} \quad \text{for} \quad t>0.$$

For this, we receive

$$H'_\lambda(t) = l(t) + \frac{\alpha(p-1)}{\lambda^p}t^{p-2},$$

where

$$l(t) = \frac{\lambda^2-t^2}{\lambda^2(1+(\frac{t}{\lambda})^2)^2} \quad \text{or} \quad l(t) = \frac{\lambda^2-t^2}{\lambda^2}\exp\left(-\frac{t^2}{2\lambda^2}\right).$$

For $t \leq \lambda$, we have $1-\frac{t^2}{\lambda^2} \geq 0$, then $H'_\lambda(t) \geq 0$.

For $t \geq \lambda$, by the condition $p \geq 1+\frac{\lambda^2}{\alpha}$, we get $\frac{\alpha(p-1)}{\lambda^{p+4}}t^{p+2} \geq \frac{t^2}{\lambda^2}$, so, $H'_\lambda(t) > 0$.

Finally, the intended result is discovered and b must be a function which is monotone. □

Now, with respect to the result regarding the presence and distinctiveness of solution of problem $(\mathcal{P})$, we prove the following conclusions.

Proposition 2.1 *With respect to a specific function $f \in L^\infty(\Omega)$ and a value of p satisfying $p \geq 1+\frac{\lambda^2}{\alpha}$, an unique solution $u \in W^{1,p}(\Omega)\cap L^\infty(\Omega)$ in a weak sense exists for problem $(\mathcal{P})$, satisfying the equation*

$$\int_\Omega u.\varphi dx + \int_\Omega (g(|\nabla u|)\nabla u + a(x,\nabla u))\,\nabla\varphi dx = \int_\Omega f.\varphi dx, \quad \forall \varphi \in W^{1,p}(\Omega). \tag{2.1}$$

Proof: For all $n \in \mathbb{N}$, (P_n) is an approximation of the problem $(\mathcal{P})$ given by

$$(P_n)\begin{cases} \displaystyle\int_\Omega u_n\varphi dx + \int_\Omega (g(|\nabla u_n|)\nabla u_n + a(x,\nabla u_n))\,\nabla\varphi dx = \int_\Omega f\varphi dxdt \quad \text{all over } \Omega, \\ (a(.,\nabla u_n) + g(|\nabla u_n|)\nabla u_n)\vec{n} = 0 \quad \text{all over } \partial\Omega, \end{cases}$$

employing the monotony method to solve an elliptic problem, we can assume that the operator represented by the following expression

$$B_n : W^{1,p}(\Omega) \to W^{1,p}(\Omega)',$$

with $< B_n u, \varphi >:= \int_\Omega b(\nabla u)\nabla\varphi dx + \frac{1}{n}\int_\Omega |u|^{p-2}u\varphi dx$ is coercive monotone (by the precedent lemma), hemicontinuous and furthermore pseudomonotone (see [3]).

Duo to [6] and [3], there is a solution just for that $u_n \in W^{1,p}(\Omega)\ \forall n \in \mathbb{N}$ so that

$$\int_\Omega u_n\varphi dx + \int_\Omega \left(g(|\nabla u_n|)\nabla u_n + a(x,\nabla u_n)\right)\nabla\varphi dx + \frac{1}{n}\int_\Omega |u_n|^{p-2}u_n\varphi dx = \int_\Omega f\varphi dx. \tag{2.2}$$

Now, taking $(u_n - ||f||_{L^\infty(Q)})^+$ like a test function within (2.2), we have

$$\int_{\Omega_1} u_n(u_n - ||f||_{L^\infty(\Omega)})^+ dx + \int_{\Omega_1} \left(g(|\nabla u_n|)\nabla u_n + a(x,\nabla u_n)\right)\nabla(u_n - ||f||_{L^\infty(\Omega)})^+ dx$$

$$+\frac{1}{n}\int_{\Omega_1} |u_n|^{p-2}u_n(u_n - ||f||_{L^\infty(\Omega)})^+ dx \leq \int_{\Omega_1} ||f||_{L^\infty(\Omega)}(u_n - ||f||_{L^\infty(\Omega)})^+ dx,$$

with $\Omega = \Omega_1 \cup (\Omega_1)^c$, $\Omega_1 = \{x \in \Omega; u_n \geq ||f||_{L^\infty(\Omega)}\}$. Then

$$\int_\Omega (u_n - ||f||_{L^\infty(\Omega)})(u_n - ||f||_{L^\infty(\Omega)})^+ \leq 0,$$

we deduce

$$(u_n - ||f||_{L^\infty(\Omega)})^+ = 0 \quad \text{a.e in} \quad \Omega. \tag{2.3}$$

In the contrary, by employing the test function $(u_n + ||f||_{L^\infty(\Omega)})^-$ in (2.2), we receive

$$\int_{\Omega_2} u_n(u_n + ||f||_{L^\infty(\Omega)})^- dx + \int_{\Omega_2} \left(g(|\nabla u_n|)\nabla u_n + a(x,\nabla u_n)\right)\nabla(u_n + ||f||_{L^\infty(\Omega)})^- dx$$

$$+\frac{1}{n}\int_{\Omega_2} |u_n|^{p-2}u_n(u_n + ||f||_{L^\infty(\Omega)})^- dx \leq -\int_{\Omega_2} ||f||_{L^\infty(\Omega)}(u_n + ||f||_{L^\infty(\Omega)})^- dx,$$

where $\Omega = \Omega_2 \cup (\Omega_2)^c$, and $\Omega_2 = \{x \in \Omega; u_n \leq -||f||_{L^\infty(\Omega)}\}$, then

$$\int_\Omega (u_n + ||f||_{L^\infty(\Omega)})(u_n + ||f||_{L^\infty(\Omega)})^- \leq 0.$$

Consequently,

$$(u_n + ||f||_{L^\infty(\Omega)})^- = 0 \quad \text{a.e in} \quad \Omega. \tag{2.4}$$

That is why we confirm by (2.3) and (2.4) the bounded solution of our approximate problem

$$||u_n||_{L^\infty(\Omega)} \leq ||f||_{L^\infty(\Omega)}.$$

$(u_n)_{(n\in\mathbb{N})}$ is bounded in $W^{1,p}(\Omega)$. Therefore, there is a subsequence that is still designated by u_n, so that $u_n \to u \in W^{1,p}(\Omega)$ in $W^{1,p}(\Omega)$. Using the standard Minty Browder in [6] the Rellich-Kondrachov theorem as well, we obtain that

$$u_n \to u \in L^p(\Omega), n \to \infty \quad \text{and} \quad ||u||_{L^\infty(\Omega)} \leq ||f||_{L^\infty(\Omega)}.$$

In that case, the solution is u to the equation that follows

$$\int_\Omega u\varphi dx + \int_\Omega \left(g(|\nabla u|)\nabla u + a(x,\nabla u)\right)\nabla\varphi dx + \frac{1}{n}\int_\Omega |u|^{p-2}u\varphi dx = \int_\Omega f\varphi dx.$$

For the uniqueness results, assuming that the equation provided in the last proposition possesses two solutions, denoted as u and u^* matching to f and f^*, in that order, then

$$\int_\Omega (u-u^*)\varphi dx + \int_\Omega \left(b(\nabla u) - b(\nabla u^*)\right)\nabla\varphi dx = \int_\Omega (f-f^*)\varphi dx \quad \forall \varphi \in W^{1,p}(\Omega). \tag{2.5}$$

Taking $L_\varepsilon(u-u^*)$ like a sign function with $\varepsilon > 0$. L_ε defined by

$$L_\varepsilon(s) := max(-1, min(\frac{s}{\varepsilon}, 1)), \quad s \in \mathbb{R}.$$

The case is then spared in two parts

for $|\frac{s}{\varepsilon}| \leq 1$, then $L_\varepsilon(u-u^*) = \frac{u-u^*}{\varepsilon}$, and we applied to (2.5), we get

$$\frac{1}{\varepsilon}\int_\Omega (u-u^*)^2 dx + \frac{1}{\varepsilon}\int_\Omega \left(b(\nabla u) - b(\nabla u^*)\right)\nabla(u-u^*)dx$$

$$= \frac{1}{\varepsilon}\int_\Omega (f-f^*)(u-u^*)dx.$$

Assuming that b is monotone prior to using the results,

$$\frac{1}{\varepsilon}\int_\Omega |u-u^*|^2 dx \leq 0, \quad \text{then} \quad u = u^*.$$

For $|\frac{s}{\varepsilon}| \geq 1$, we have $L_\varepsilon(u-u^*) = sign(u-u^*)$, and $\nabla L_\varepsilon(u-u^*) = 0$.
Then

$$\int_\Omega |u-u^*|dx \leq 0.$$

□

Finlay, we have the desired unique solution for our problem $(\mathcal{P})$.

3. Asymptotic behavior $p \to \infty$

This section looks at the way in which the answer to problem $(\mathcal{P})$ behaves as p approaches infinity. To achieve this, we examine the asymptotic properties. Also for facilitate our analysis, we introduce the concept of a closed convex set denoted as K_λ, which defined by

$$K_\lambda = \{\Phi \in W^{1,p}(\Omega) : |\nabla\zeta| \leq \lambda \quad \text{a.e. in } \Omega\}.$$

Theorem 3.1 *As p tends to infinity, let $f \in L^\infty(\Omega)$ and u_p represent the weak solution of problem $(\mathcal{P})$. For all $q > 0$, u_p converges weakly to u in $W^{1,q}(\Omega)$ as $p \to \infty$, where u represents the only solution meeting the subsequent requirements: $u \in K_\lambda$ and*

$$\int_\Omega u(u-\Phi)dx + \int_\Omega g(|\nabla u|)\nabla u\nabla(u-\Phi)dx \leq \int_\Omega f(u-\Phi)dx \quad \forall \Phi \in K_\lambda. \tag{3.1}$$

Proof:
After integrating over Ω and multiplying $(\mathcal{P})$ by u_p, we obtain

$$\int_\Omega u_p^2 dx + \int_\Omega g(|\nabla u_p|)|\nabla u_p|^2 + \int_\Omega a(x, \nabla u_p)\nabla u_p = \int_\Omega f u_p,$$

we obtain by (1.4) that

$$\int_\Omega f u_p dx \geq \alpha \int_\Omega \left|\frac{\nabla u_p}{\lambda}\right|^p dx,$$

then

$$\int_\Omega \left|\frac{\nabla u_p}{\lambda}\right|^q dx \leq \frac{1}{\alpha}||f||_{L^\infty(\Omega)}.||f||_{L^1(\Omega)}.$$

And we now

$$\int_\Omega \left|\frac{\nabla u_p}{\lambda}\right|^q dx = \int_{\{|\nabla u_p \leq \lambda|\}} \left|\frac{\nabla u_p}{\lambda}\right|^q dx + \int_{\{|\nabla u_p \geq \lambda|\}} \left|\frac{\nabla u_p}{\lambda}\right|^q dx.$$

For $q < p$, we get

$$\begin{aligned}\int_\Omega \left|\frac{\nabla u_p}{\lambda}\right|^q dx &= \int_{\{|\nabla u_p \leq \lambda|\}} \left|\frac{\nabla u_p}{\lambda}\right|^q dx + \int_{\{|\nabla u_p \geq \lambda|\}} \left|\frac{\nabla u_p}{\lambda}\right|^p dx,\\ &\leq |\Omega| + \frac{1}{\alpha}||f||_{L^\infty(\Omega)}.||f||_{L^1(\Omega)}.\end{aligned}$$

Following that, we can write

$$||\frac{u_p}{\lambda}||^q_{W^{1,q}(\Omega)} \leq \frac{|\Omega|}{\lambda^q}||f||^q_{L^\infty(\Omega)} + |\Omega| + \frac{1}{\alpha}||f||_{L^\infty(\Omega)}||f||_{L^1(\Omega)}.$$

And, we give

$$||u_p||_{W^{1,q}(\Omega)} \leq ||f||_{L^\infty(\Omega)}.|\Omega|^{\frac{1}{q}} + \lambda\left(|\Omega| + \frac{1}{\alpha}||f||_{L^\infty(\Omega)}||f||^{\frac{1}{q}}_{L^1(\Omega)}\right).$$

We obtain, $(u_p)_{p\in\mathbb{N}} \in W^{1,q}(\Omega)$, implying that a weak limit $u \in W^{1,q}(\Omega)$ of a sub-sequence u_p exists, with $u_p \to u \in W^{1,q}(\Omega)$ additionally, we write when $p \to \infty$

$$u_p \to u \in L^q(\Omega).$$

We now need to demonstrate that $u \in K_\lambda$. To do this, we can use the convexity of $||.||_{L^q(\Omega)}$ to show that

$$\int_\Omega \left|\frac{\nabla u}{\lambda}\right|^q dx \leq \liminf_{p\to\infty} \int_\Omega \left|\frac{\nabla u_p}{\lambda}\right|^q dx \leq |\Omega| + \frac{1}{\alpha}||f||_{L^\infty(\Omega)}||f||_{L^1(\Omega)}, \quad \forall q > 1.$$

For $\tau > 1$

$$\mu(\{\left|\frac{\nabla u}{\lambda}\right| \geq \tau\}) = \frac{1}{\tau^q}\int_{\{|\frac{\nabla u}{\lambda}|\geq\tau\}} \tau^q \leq \frac{|\Omega| + \frac{1}{\alpha}||f||_{L^\infty(\Omega)}||f||_{L^1(\Omega)}}{\tau^q}.$$

For $q \to \infty$, we get $\mu\{(|\frac{\nabla u}{\lambda}| \geq \tau)\} = 0$.
Then, we take $u_p - \varphi$ with $\varphi \in K_\lambda$ as a function under test in $(\mathcal{P})$, we get

$$\int_\Omega u_p(u_p - \varphi) + \int_\Omega b(\nabla u_p)\nabla(u_p - \varphi) = \int_\Omega f(u - \varphi),$$

by letting $p \to \infty$, we get

$$\int_\Omega u(u - \varphi) + \liminf_{p\to\infty} \int_\Omega b(\nabla u_p)\nabla(u_p - \varphi) = \int_\Omega f(u - \varphi),$$

we must establish the inequality

$$\liminf_{p\to\infty} \int_\Omega b(\nabla u_p)\nabla(u_p - \varphi) \geq \int_\Omega g(|\nabla u|)\nabla(u - \varphi).$$

Taking $\tau \in (0,1)$ and applying the function's monotonicity, then

$$\begin{aligned}\int_\Omega b(\nabla u_p)\nabla(u_p-\tau\varphi) &= \int_\Omega (b(\nabla u_p)-b(\tau\nabla\varphi))\nabla(u_p-\tau\varphi)+\int_\Omega b(\tau\nabla\varphi)\nabla(u_p-\tau\varphi)\\ &\geq \tau\int_\Omega g(|\tau\nabla\varphi|)\nabla\varphi\nabla(u_p-\tau\varphi)+\int_\Omega a(x,\tau\nabla\varphi)\nabla(u_p-\tau\varphi)\\ &\geq \tau\int_\Omega g(|\tau\nabla\varphi|)\nabla\varphi\nabla(u_p-\tau\varphi)-\int_\Omega a(x,\tau\nabla\varphi)\nabla(\tau\varphi-u_p)\\ &\geq \tau\int_\Omega g(|\tau\nabla\varphi|)\nabla\varphi\nabla(u_p-\tau\varphi)-\frac{\alpha}{\lambda^p}\tau^{p-1}\int_\Omega |\nabla\varphi|^{p-1}|\nabla(\tau\varphi-u_p)|\end{aligned}$$

and, we now $\varphi \in K_\lambda$ that is why $\left|\frac{\nabla\varphi}{\lambda}\right| \leq 1$ a.e in Ω, then

$$\lim_{p\to\infty}\frac{\alpha}{\lambda}\tau^{p-1}\int_\Omega \left|\frac{\nabla\varphi}{\lambda}\right|^{p-1}\nabla(u_p-\tau\varphi)=0.$$

Letting $p\to\infty$ and $\tau\to 1$, we get

$$\lim_{p\to\infty}\int_\Omega b(\nabla u_p)\nabla(u_p-\varphi)\geq\lim_{p\to\infty}\int_\Omega g(|\nabla\varphi|)\nabla\varphi\nabla(u_p-\varphi)=\int_\Omega g(|\nabla\varphi|)\nabla\varphi\nabla(u-\varphi).$$

And, we take $\varphi = tu+(1-t)v$, with $t\in(0,1)$ and $v\in K_\lambda$.

$$\lim_{p\to\infty}\int_\Omega b(\nabla u_p)\nabla(u_p-(tu+(1-t)v)))\geq(1-t)\int_\Omega g(|t\nabla u+(1-t)\nabla v|)\nabla(u-v), \tag{3.2}$$

however, we also have

$$\int_\Omega \frac{b(\nabla u_p).\nabla(u_p-(tu+(1-t)v)))}{1-t}=\frac{t}{1-t}\int_\Omega b(\nabla u_p)\nabla(u_p-u)+\int_\Omega b(\nabla u_p)\nabla(u_p-v).$$

By letting $p\to\infty$, we get

$$\lim_{p\to\infty}\int_\Omega \frac{b(\nabla u_p)\nabla(u_p-(tu+(1-t)v)))}{1-t}=\lim_{p\to\infty}\int_\Omega b(\nabla u_p)\nabla(u_p-v).$$

Return to the inequality (3.2), with g continuous and bounded

$$\lim_{p\to\infty}\int_\Omega g(|t\nabla u+(1-t)\nabla v|)\nabla(u-v)=\int_\Omega g(|\nabla u|)\nabla(u-v).$$

Then,

$$\liminf_{p\to\infty}\int_\Omega b(\nabla u_p)\nabla(u_p-v)\geq\int_\Omega g(|\nabla u|)\nabla(u-v).$$

□

Now, present the solution's distinctness, assume that u and u^* two solutions of $(\mathcal{P})$ for the inequality (3.1). By using u and u^* like two function tests in the inequality that is met by the solutions u respectively u^*, after we adding the two inequality's to obtain

$$\int_\Omega (u-u^*)^2+\int_\Omega (b(\nabla(u)-b(\nabla u^*))\nabla(u-u^*)\leq 0.$$

Such that b is monotone for u, u^* in K_λ, then

$$\int_\Omega (u-u^*)^2\leq 0,$$

we get that $u=u^*$ pp in Ω in the norme of $L^2(\Omega)$.

Remark 3.1 Employing the identical technique for the evolution equation linked to our issue $(\mathcal{P})$, as provided by

$$u_t - \frac{1}{\lambda^p}\text{div}\, a(x,\nabla u) - \text{div}\,(g(|\nabla u|)\nabla u) = f - u \quad \text{in } Q.$$

Setting aside traditional results (see [13]),

$$\mathcal{W} = \{\varphi \in L^p(0,T;W^{1,p}(\Omega)) : \frac{\partial \varphi}{\partial t} \in L^{p'}(0,T;(W^{1,p}(\Omega))'), \quad p>1\}. \tag{3.3}$$

Then, we get $\mathcal{W} \subset \mathcal{C}([0,T];L^2(\Omega))$.
The precedent lemma 2.2 should be applied to the stationary issue as well as Lions theory [13] can demonstrate that the problem in (3.3) has a special weak solution as well u_p. Furthermore, when $p \to \infty$ we obtain

$$u_p \to u \quad \text{weakly in} \quad L^p(0,T;W^{1,p}(\Omega)), \quad p>1.$$

And, in the asymptotic behavior we can write that

$$\int_0^T < \frac{\partial u}{\partial t}, u-\varphi > dt + \int_0^T \int_\Omega g(|\nabla u|)\nabla u \nabla(u-\varphi) \leq \int_0^T < f-u, u-\varphi >,$$

where, $u \in \mathcal{W} \cap \mathcal{K}_t^\lambda$ the unique solution for this inequality, and

$$\varphi \in K_t^\lambda = \{\zeta \in L^p(0,T;W^{1,p}(\Omega)) : \zeta(t) \in \mathcal{K}_\lambda\}.$$

4. Numerical results

For our numerical results, we take the following model noted RPM (Regularised Perona-Malik), with distinct Carathéodory function as observed by $a_i(x,\zeta)$, $i=\{1,2,3\}$ into account

$$\begin{cases} u_t - \text{div}\,(g(|\nabla u|).\nabla u + a_i(x,\nabla u)) = 0 \quad \text{in } Q, \\ (a_i(.,\nabla u) + g(|\nabla u|)\nabla u).\vec{n} = 0 \quad \text{in } \partial Q, \\ u_0(x) = f \quad \text{in } \Omega. \end{cases}$$

Where $Q := \Omega \times (0,T) \subset \mathbb{R}^2 \times (0,T)$.

To derive numerical solutions, we discretize the set of formulas containing temporal and spatial variables. Subsequently, we employ the finite difference method [19] to solve the resulting discretized system. This approach involves representing the image $u(x,y)$ as a discretized grid of pixel intensities (r,s) located at (x_r, y_s), where $r=1,\ldots,N$ and $s=1,\ldots,M$. Determines the resolution of the discretized image. Additionally, by employing a time step of Δt, the pixel (r,s) at a particular discrete time. $t_n = n \cdot \Delta t$ is referred to as $U^n(r,s)$. The gradient and divergence of the image $U^n(r,s)$ is computed as follows:

$$\begin{array}{ll} \nabla_x^+ U_{r,s}^n = U_{r+1,s}^n - U_{r,s}^n, & \nabla_x^- U_{i,j}^n = U_{r,s}^n - U_{r-1,s}^n, \\ \nabla_y^+ U_{r,s}^n = U_{r,s+1}^n - U_{r,s}^n, & \nabla_y^- U_{r,s}^n = U_{r,s}^n - U_{r,s-1}^n. \end{array}$$

where $\nabla U^n(r,s) = [\nabla_x^+ U_{r,s}^n, \nabla_y^+ U_{r,s}^n]$ and $\text{div}\, X^n(r,s) = [\nabla_x^- X_{r,s}^n, \nabla_y^- X_{r,s}^n]$
The Euler technique in explicit form is given as

$$U^{n+1}(r,s) = U^n(r,s) + dt * div\left(a((r,s),\nabla U^n(r,s))|\nabla U^n(r,s)|^{p-2}\nabla U^n(r,s)\right), \tag{4.1}$$

where $U^0(r,s))$ symbolizes the noisy image, and $U^{n+1}(r,s)$ represents the denoised image in the $n+1$ iteration.

Figure 2: Compare the restored images using the differents following models: (a) the initial and noisy images, (b) the PM filter, (c) the PMPL filter, (d) the RPM1 filter and (e) the RPM2 filter, with a fixed parameter $\lambda = 10$ and p changed.

Regarding every numerical simulation that this work presents, we'll offer for $dt = 0.0002$ and 10^3 iterations. The restoration of the Lena image is depicted in Figure 2 for two well-known models in the field, the PM (Perona-Malik) model and the PMPL (Perona-Malik combined by p-Laplacian operator) model treated in [3] and our model utilized in this study, was achieved by utilizing a_1 and a_2 the first and second Carathéodory functions provided in the introduction, denoted by RPM1 and RPM2, respectively, where the first regularization parameter p has two distinct values, $p = 8$ and $p = 10$, while the second regularization parameter $\lambda = 15$ is fixed. In contrast, Figure 4 shows the restored image obtained using the following models PM, PMPL, the work's particular model RPM1, and RPM2 with regularization parameter $p = 8$ and different λ values, $\lambda = 8$ and $\lambda = 10$.

An effective visual comparison of our RPM3 (Regularised Perona-Malik 3) model attained by using the third Carathéodory function given in the beginning is shown in figure 3, the PM (Perona-Malik) and PMPL (Perona-Malik combined with p-Laplacian operator) models. To determine the optimal parameters of our model and demonstrate its effectiveness compared to the PM and PMPL using various models, we compute the PSNR (Peak Signal-to-Noise Ratio) of the restored images. This comparative analysis will allow us to select optimal parameters for our model and demonstrate its effectiveness compared to the PM and PMPL models in terms of image restoration quality.

The table 1 displays the PSNR values of the Lena image from figures 1 and 2 for various values of λ and p.

Image	Lena image (Figure2)		Moon image (Figure4)	
Parametrs	p=8	p=10	$\lambda = 10$	$\lambda = 15$
Noisy image	19,4944	19,5111	11,9702	11,9702
PM model	22,9972	22,8340	11.6628	11.6619
PMPL model	23,1072	23,8087	11.8859	12.1635
RPM1 model	23,6228	23,8268	12,1872	12,9210
RPM2 model	23,3984	23,3159	12,2648	12,4274

Table 1: PSNR values for different models.

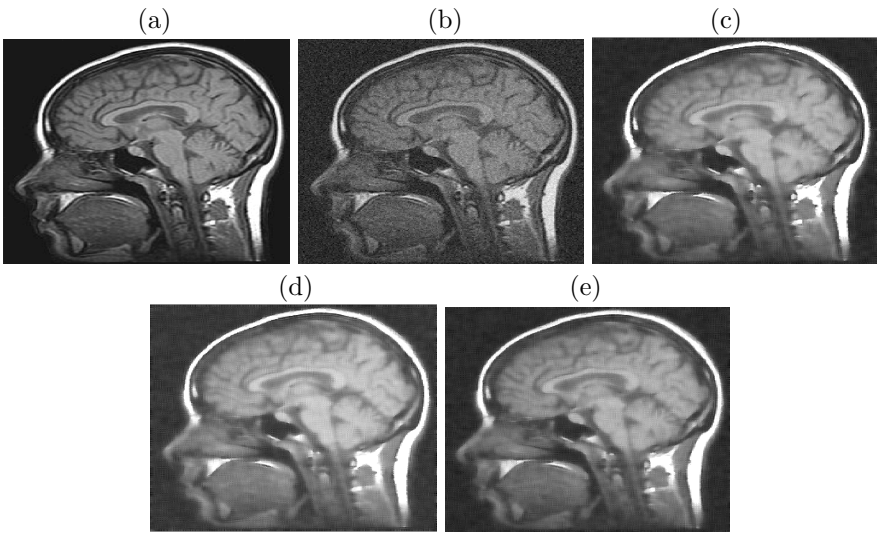

Figure 3: The restored images using the PM and PMPL and RPM3 models to the following: (a) the initial image, (b) the noisy image, (c) the restored image using the PM filter, (d) the restored image using the PMPL filter, and (e) is produced by our PMR3 model.

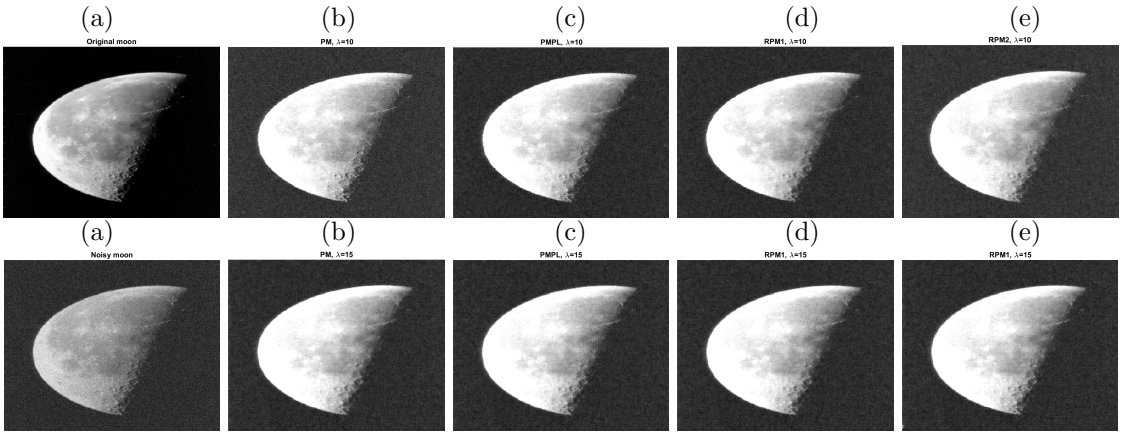

Figure 4: Compare the restored images using the differents following models: (a) the initial and noisy images, (b) the PM filter, (c) the PMPL filter, (d) the RPM1 filter and (e) the RPM2 filter, with a fixed parameter $p = 8$ and λ changed.

5. Conclusion

In this research, we revisited the Perona-Malik model, renowned for its edge-preserving smoothing capabilities, but identified significant limitations such as the "paradoxical result" and the "staircase effect," which affect the quality of denoised images. To overcome these challenges, we proposed extending the Perona-Malik framework by replacing the conventional p-Laplacian operator with a more adaptable Leray-Lions type operator. Our rigorous theoretical analysis using the monotonicity method confirmed the existence and uniqueness of weak solutions under suitable growth, coercivity, and monotonicity conditions. This foundational work paves the way for further enhancements in image denoising techniques. In the numerical tests, our model outperformed the Perona-Malik model that incorporates the p-Laplacian operator. Our regularized Perona-Malik (RPM) model not only mitigates the staircase effect but also maintains fine details in images and produces an efficient restoration result without condition on p or λ, demonstrating a notable enhancement in image quality. The results from experiments using various Carathéodory functions validate the model's effectiveness and versatility in different situations. Overall, incorporating the Leray-Lions operator into the Perona-Malik framework offers a significant improvement in image denoising methods. This approach effectively mitigates key issues previously encountered and achieves superior image quality. This progress underscores the need for ongoing innovation in the field. Future research is expected to extend these results by refining denoising techniques, possibly integrating more advanced computational methods and exploring further regularization approaches to address new challenges in digital image processing.

Conflict of Interests

The authors declare that they have no conflict of interests.

References

1. Aboulaich, R., Meskine, D. and Souissi, A., 2008. *New diffusion models in image processing.* Computers and Mathematics with Applications, 56(4), pp.874-882.

2. Amann, H., 2007. *A time-delayed Perona-Malik type problems.* Proceedings of Equadiff 11, pp.15-38.

3. Atlas, A., Karami, F. and Meskine, D., 2014. *The Perona-Malik inequality and application to image denoising.* Nonlinear Analysis: Real World Applications, 18, pp.57-68.

4. Aubert, G. and Kornprobst, P., 2006. *Mathematical problems in image processing: partial differential equations and the calculus of variations.* Springer; New York etc., 2nd ed.

5. Ben-Loghfyry, A. and Charkaoui, A., 2023. *Regularized Perona & Malik model involving Caputo time-fractional derivative with application to image denoising.* Chaos, Solitons & Fractals, Vol. 175, Part 1, 113925.

6. Brezis, H., 1968. *Equations et inéquations non linéaires dans les espaces vectoriels en dualité.* In Annales de l'institut Fourier, Vol. 18, No. 1, pp. 115-175.

7. Buades, A., Coll, B. and Morel, J.M., 2005, June. *A non-local algorithm for image denoising.* In 2005 IEEE computer society conference on computer vision and pattern recognition (CVPR'05), Vol. 2, pp. 60-65.

8. Catté, F., Lions, P.L., Morel, J.M. and Coll, T., 1992. *Image selective smoothing and edge detection by nonlinear diffusion.* SIAM Journal on Numerical analysis, 29(1), pp.182-193.

9. Chan, T.F. and Shen, J., 2005. *Image processing and analysis: variational, PDE, wavelet, and stochastic methods.* Society for Industrial and Applied Mathematics.

10. Chen, Y., Levine, S. and Rao, M., 2006. *Variable exponent, linear growth functionals in image restoration.* SIAM journal on Applied Mathematics, 66(4), pp.1383-1406.

11. Kbiri Alaoui, M., Nabil, T., Altanji, M., 2014. *On some new non-linear diffusion models for the image filtering.* Applicable Analysis, 93(2), pp. 269-280.

12. Kichenassamy, S., 1997.*The Perona–Malik paradox.* SIAM Journal on Applied Mathematics, 57(5), pp.1328-1342.

13. Lions, J.L., 1969. *Quelques methodes de resolution des problemes aux limites non lineaires.* Dunford/Gauthier-Villars.

14. Mairal, J., Bach, F., Ponce, J., Sapiro, G. and Zisserman, A., 2009, September. *Non-local sparse models for image restoration.* In 2009 IEEE 12th international conference on computer vision, pp. 2272-2279.

15. Perona, P. and Malik, J., 1990. *Scale-space and edge detection using anisotropic diffusion.* IEEE Transactions on pattern analysis and machine intelligence, 12(7), pp.629-639.

16. Rudin, L.I., Osher, S. and Fatemi, E., 1992. *Nonlinear total variation based noise removal algorithms.* Physica D: nonlinear phenomena, 60(1-4), pp.259-268.

17. Weickert, J., 1998. *Anisotropic diffusion in image processing* (Vol. 1, pp. 59-60). Stuttgart: Teubner.

18. Zhang, L., Dong, W., Zhang, D. and Shi, G., 2010. *Two-stage image denoising by principal component analysis with local pixel grouping*. Pattern recognition, 43(4), pp.1531-1549.

19. Marin, M., Hobiny, A. and Abbas, I., 2021. *Finite element analysis of nonlinear bioheat model in skin tissue due to external thermal sources*. Mathematics, 9(13): 1459.

S.M. Douiri,
IMIA Laboratory, A2MSDS Group, Department of Mathematics,
Faculty of Sciences and Technics, Moulay Ismail University of Meknes,
P.O. Box 509 Boutalamine, Errachidia 52000, Morocco.

and

H. Farjil,
IMIA Laboratory, A2MSDS Group, Department of Mathematics,
Faculty of Sciences and Technics, Moulay Ismail University of Meknes,
P.O. Box 509 Boutalamine, Errachidia 52000, Morocco.
E-mail address: hindfarjil@gmail.com

and

M. Moumni,
MAMCS Group, Department of Mathematics,
Faculty of Sciences and Technics, Moulay Ismail University of Meknes,
P.O. Box 509 Boutalamine, Errachidia 52000, Morocco.